doi:10.1038/nature10178

Supplementary Table 1

Data Collection Statistics	BL-bound BRI1-LRR	Free BRI1-LRR
Beam Line	Beam line BL17U1, SSRF	
Space Group	C2	C2
Wavelength (Å)	1.0	1.0
Number of Reflections	49,788 (5,066)	41,987 (4,152)
Cell dimensions		
a, b, c (Å)	170.41, 66.82, 114.34	173.391, 66.705 119.051
α, β, γ (°)	90.00, 119.50, 90.00	90.00 120.98 90.00
Resolution (Å)	2.28(2.36-2.28)	2.47(2.56-2.47)
R_{sym} (%)	5.6(20.4)	7.8(58.5)
$I/\sigma(I)$	21.4(5.9)	30.0(2.7)
Completeness (%)	97.2(99.7)	99.5(98.4)
Redundancy	3.2(3.2)	4.0(3.8)
Refinement Statistics		
Resolution (Å)	50.0-2.28(2.32-2.28)	50.0-2.47(2.53-2.47)
No. Reflections	49,782 (2,596)	41,889 (2,601)
Rwork/Rfree %	18.2/21.2(18.96/24.1)	22.0/26.3(32.3/37.8)
Number of BRI1-LRR molecules/asymmetric unit	1	1
Protein all atoms	5654	5574
Non-protein atoms	595	315
All non-hydrogen atoms	6249	5889
Averaged B factor of protein atoms	41.0	64.6
Averaged B factor of BL	44.3	
R.m.s deviations		
Bond Lengths (Å)	0.007	0.009
Bond Angles (°)	1.212	1.295
Ramachandran (%) (from COOT)		
Preferred region	91.23	90.45
Allowed region	8.5	9.0
Outliers	0.27	0.55

Highest resolution shell is shown in parenthesis

*The occupancies of all BL atoms were fixed at 1.0 and subsequently subjected to B-factor refinement together with other parameters.

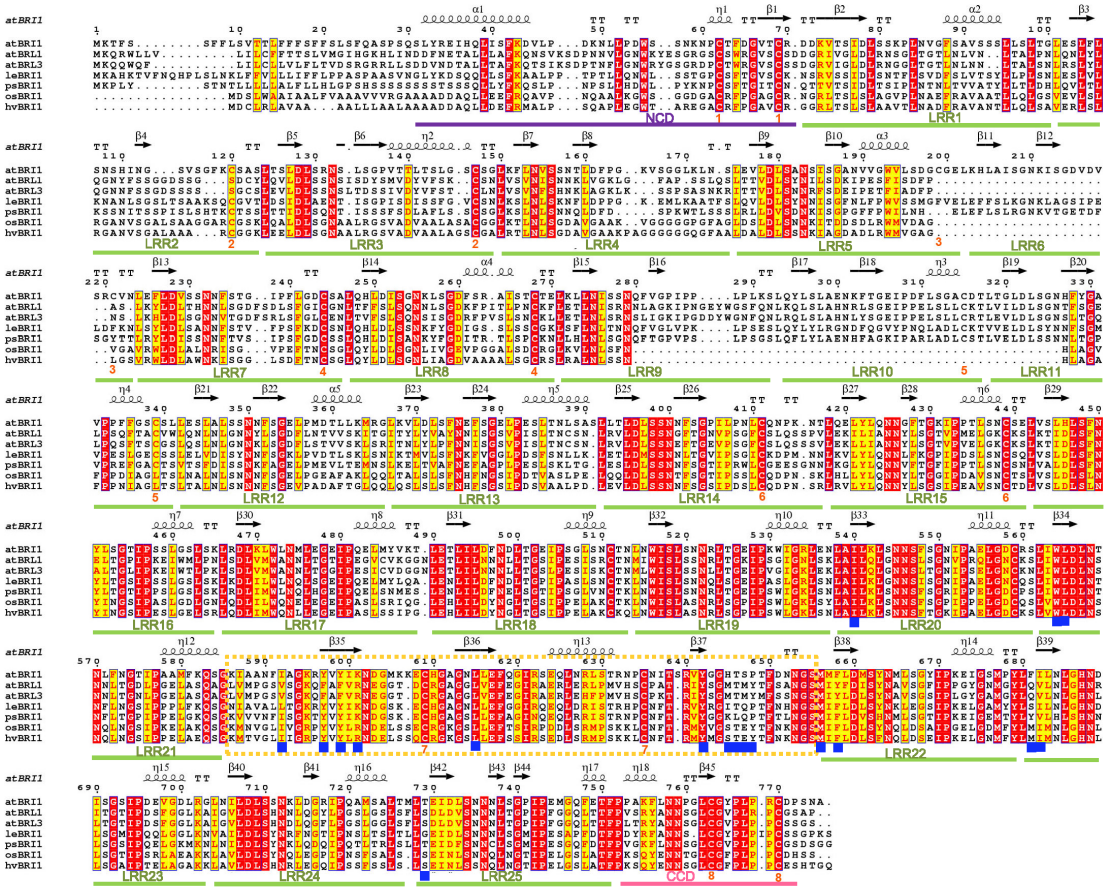

Fig. 1 **Sequence alignment of ectodomain BRI1 among different species**

Conserved and similar residues are highlighted with red and yellow grounds respectively. The ID is highlighted within the light orange dashed square. Residues involved in BL recognition are indicated with blue solid squares at bottom. Two cysteines that form a disulfide bond are indicated by the same orange number at bottom. "NCD" and "CCD" represent the N-terminal and C-terminal capping domain respectively. "at", "le", "ps", "os" and "hv" represent *Arabidopsis*, *Solanum lycopersicum*, *Oryza sativa*, *Pisum sativum* and *Hordeum vulgare* , respectively.

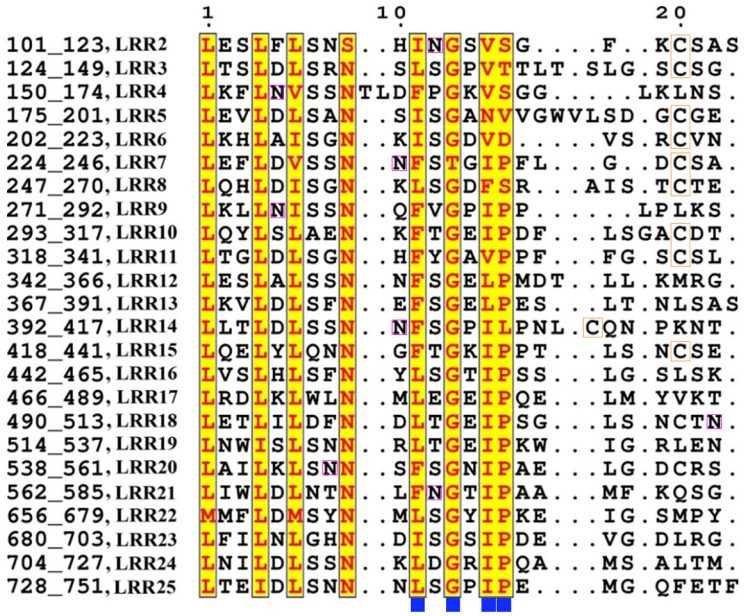

Fig. 2 **Sequence alignment of regular LRRs in BRI1**

The boundary of each LRR and its numbering are shown on the left side. The conserved residues are shown with yellow background. Cysteines forming disulfide bonds and glycosylated asparagines are highlighted with orange and magenta squares respectively. The residues from the plant-specific motif in the LRRs are highlighted with blue solid squares at the bottom.

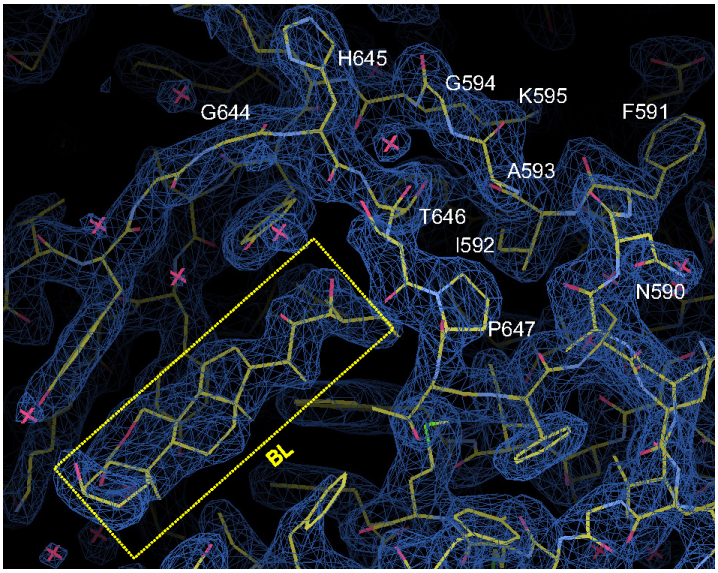

Fig 3 **Electron density around the inter-domain loops in BR-bound BRI1-LRR**
Electron density (2Fo-Fc) contoured at 1.30 sigma (under COOT) around the inter-domain loops. The residues from the loops are labeled in white. BL is highlighted within the yellow dashed frame.

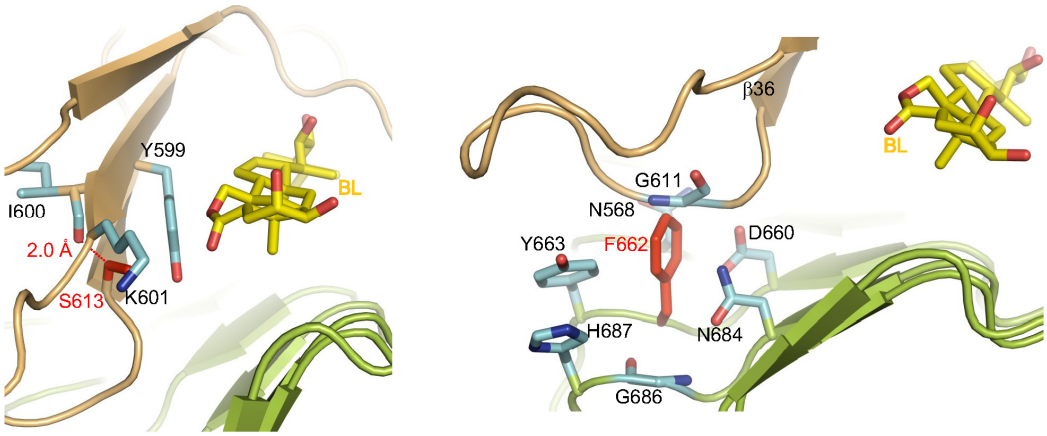

Fig 4 **Modeling of the genetic mutants G613S and S662F of BRI1-LRR**
Shown on the left and right are close-up views of the area surrounding G613S and S662F respectively. Gly613 and Ser662 were mutated to serine and phenylalanine respectively under the program COOT. The side chains of these two residues are shown in red and all the others in cyan. BL is shown yellow and stick. In the modeled structure, the Cβ atom of S613 (on the left) is 2.0 Å from the carbonyl oxygen of Ile600, whereas the minimum distance between the benzene ring of Phe662 and the amide nitrogen of Gly611 is less than 1.5 Å (right panel).

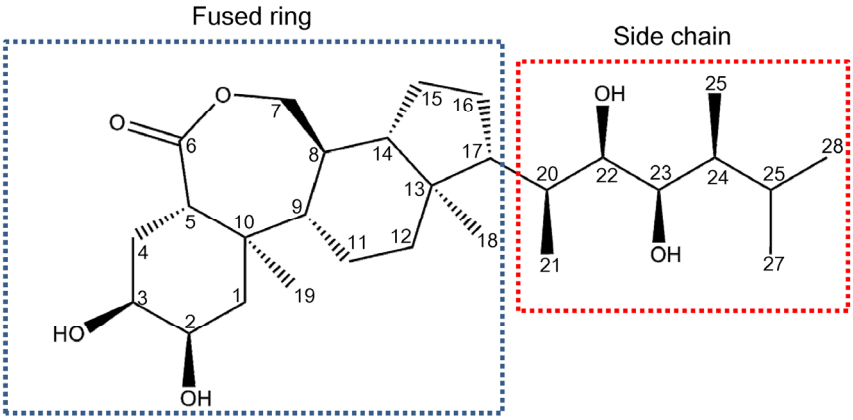

Fig. 5 **Chemical structure of BL**

The carbon atoms are labeled as indicated. The side chain and fused ring portions are highlighted in red and blue dashed frames, respectively.

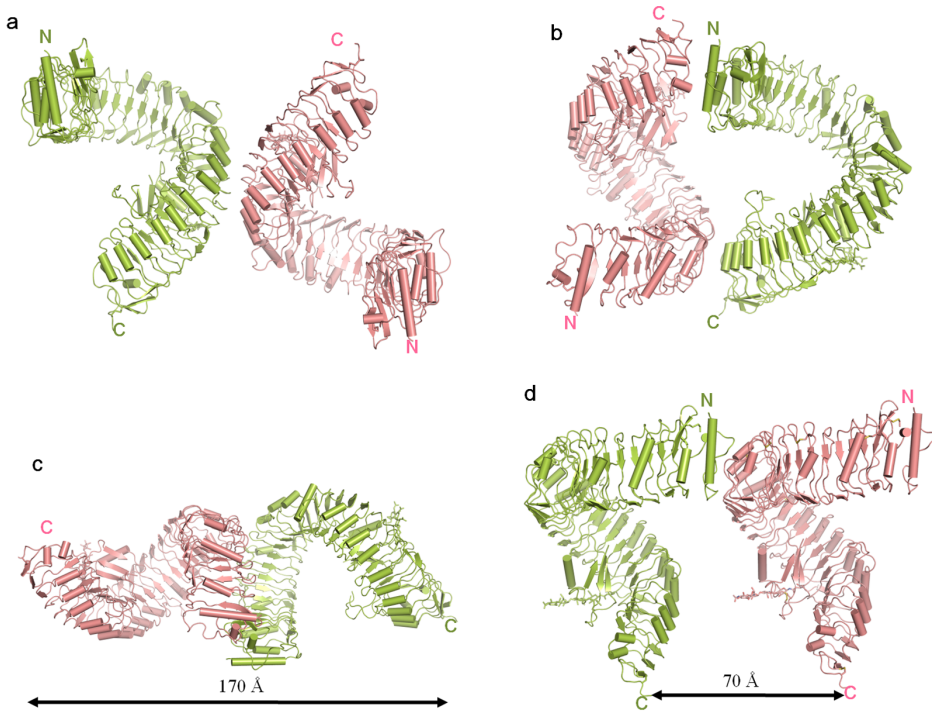

Fig. 6 **Packing of BRI1-LRR (BL-bound) with its symmetry-related neighboring molecules in crystals**

(**a**), (**b**), (**c**) and (**d**) are dimers formed by two crystallographic symmetry-related monomers of BRI1-LRR. Two monomers are colored in salmon and limon and their N- and C-terminus are indicated.

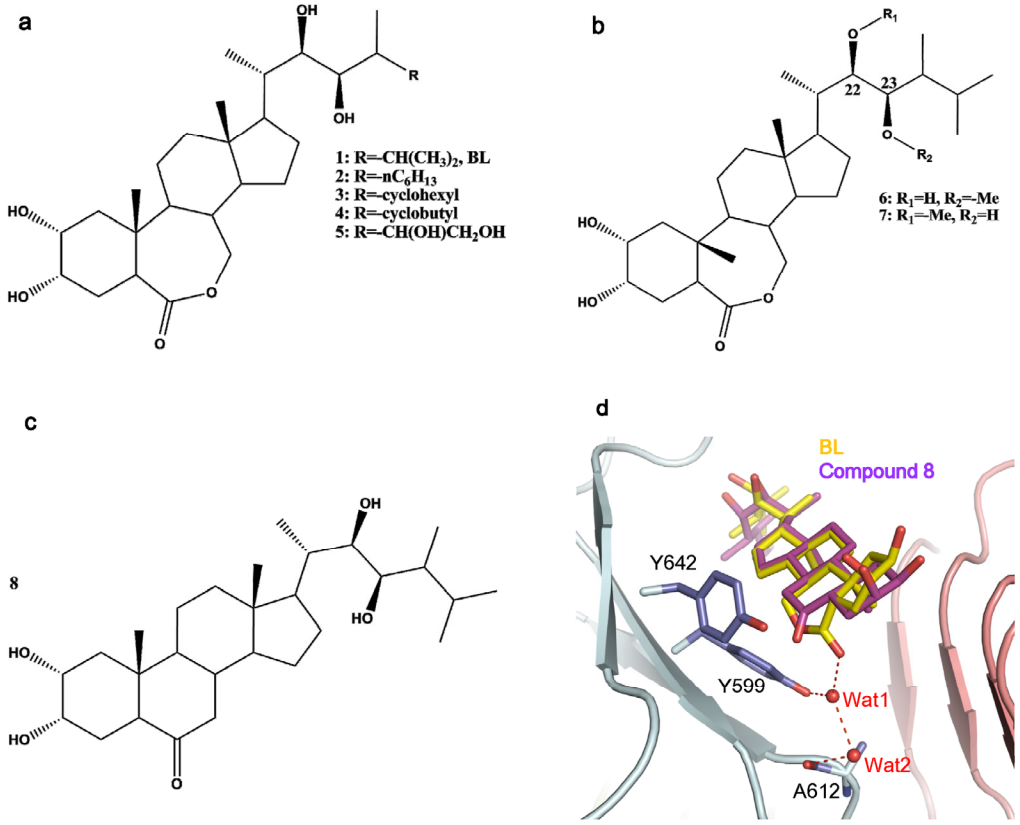

Fig. 7 **Structural basis for structure-activity relationship of BL derivatives**

a. BL derivatives with different groups at the end of side chain. One structural feature of the active BRs is their hydrophobic end of the side chain[1], which binds an exclusively hydrophobic pocket in the structure of BL-bound BRI1-LRR (Fig. 3b and Fig. 4c). Thus, removal of this moiety or introduction of polar substituents (compound 5) significantly attenuates BR binding activity[1]. A limited volume of the pocket greatly circumscribes the size of a group at this position. BL derivatives carrying a larger group such as n-C_6H_{13} (compound 2) or cyclohexyl group (compound 3) at this position exhibited little bioactivity[2]. In contrast, substitutions with functional groups like cyclobutyl (compound 4) that can better fit into the pocket resulted in more potent derivatives.

b. Molecular formula of BL derivatives with methylation of the hydroxyl group at C23 or C22. The hydroxyl group at C23 forms hydrogen bonds with BRI1-LRR (Fig. 3b), providing an explanation for the observation that methylation at this position (compound 6) produced a much more deleterious effect on the bioactivity of BR than at C22 (compound 7)[1].

c. Molecular formula of a BL derivative with a six-atom B ring. The bioactivity of this compound is about 10% of that of BL[1].

d. A model of compound 8 in complex with BRI1-LRR. The side chains of BRI1-LRR were shown in slate. Hydrogen bonds are represented in red dashed lines. Modeling study was performed using the program Auto-Dock4.2 (ref. 3). The calculated binding energy for BL and compound 8 to BRI1-LRR was -13.4 kcal/mol and -12.7 kcal/mol respectively. A lower calculated binding affinity between BRI1-LRR and compound 8 could result from a weaker hydrogen bond (with a distance of 3.4 Å as compared to 2.9 Å in BRI1-LRR/BL complex) between the oxo and the water (Wat1) molecule, which in turn makes a water (Wat2)-mediated hydrogen bond with the carbonyl oxygen of Ala612.

References

1. Zullo, M.T.A & Adam, G. Brassinosteroid phytohormones-structure, bioactivity and applications. Braz. J. Plant Physiol. 14, 143-181 (2002).
2. Back, T. G. & Pharis, R. P. Structure-Activity Studies of Brassinosteroids and the Search for Novel Analogues and Mimetics with Improved Bioactivity. J Plant Growth Regul 22, 350-361 (2003).
3. Trott, O., & Olson, A. J. AutoDock Vina: improving the speed and accuracy of docking with a new scoring function, efficient optimization and multithreading, J Comput Chem. 31, 455-61 (2010).